Formation of thermal oxide scale and its adhesion to hot-rolled low carbon steels with different final strip thicknesses

Sun Naipinij, *Sasapan* Sukieum, *Ravinupha* Namprai, and *Thanasak* Nilsonthi*

High Temperature Corrosion Research Centre and Department of Materials and Production Technology Engineering, Faculty of Engineering, King Mongkut's University of Technology North Bangkok, 1518, Pracharat 1 Road, Wongsawang, Bangsue, Bangkok, 10800, Thailand

Abstract. Currently, the steelmaking industry produces iron oxide waste scale resulting in pollution to the environment. It was necessary to have a good understanding of the composition, characteristics and properties of the oxide scale. This study focused on the formation of scale and its adhesion to the hot-rolled steel strip with different thicknesses. The oxide scale formed on an as-received hot-rolled steel strip was investigated by X-ray diffraction (XRD), scanning electron microscopy equipped with energy dispersive X-ray (SEM-EDS). Magnetite, hematite and iron were found from the XRD results of all samples, which had the thickness strip of 8, 10 and 12 mm. The scale was thinner for the thinner strip. The adhesion test was conducted by a tensile testing machine adapted with an observation set. The strain initiating the first spallation and mechanical adhesion energy was lowest for the sample with the highest thickness (12 mm). These results indicate that the waste scale produced by hot rolled steel industry can be controlled by the final strip thickness. There was a need to control the scale of waste in a reasonable way to protect the environment.

Keyword. Waste scale, Iron oxide, Rolling mill steel, Hot-rolled steel, Strip thickness, Adhesion

1 Introduction

The thermal oxide scale formed on the steel surface because of the process temperature in the hot rolling line, which is around 600-1250°C. It is de-scaled both, first before the slab enters the roughing mill and again before the steel bar enters the finishing mill, using a high-pressure water jet. Thermal oxide scale continues to rapid form during steel strip coiling and storage after the second de-scaling, until the temperature decreases below 400°C. The existence of this scale has a significant impact on the product's quality.

A slab is a raw material for making carbon steel strips in a hot rolling line, and it can be made in one of two ways: blast furnace (BF) or electric arc furnace (EAF). A blast-furnace route can be used to make a slab from iron ore, coal, and limestone. For the electric arc furnace route, steel scraps are the main raw material for making a slab, tramp elements in steel were present in the slab and might affect the thermal oxide scale structure. This may have an impact on the pickling behaviour in the following pickling line.

During the hot rolling process, steel is oxidised and a scale of iron oxide formed on the steel surface at process temperature comprises three layers a thin outermost hematite (Fe_2O_3), an intermediate magnetite (Fe_3O_4), and a thick inner wustite (FeO) [1-13]. For the Fe-O system, the scale layer can vary via concentration gradients of oxygen. An iron oxide formed always grows external scale rather than forming internal oxidation. Due to eutectoid decomposition during cooling, magnetite can be occasionally found in the wustite layer. The hematite layer may also be absent in some cases.

In the hot rolling process, a slab is rolled at high temperatures in order to obtain a strip with desired thickness [14]. At high temperatures, the steel reacts with oxygen in the ambient atmosphere and gives a thermal oxide scale [1-13]. The oxide formed is a waste of the process and it should be minimised. Many factors can affect the amount of the scale formation, such as alloying elements in the steel like C [15], Si [16], Cu [17], Sn [18] or Ti and Nb [19] or the parameters set in the process [20-22]. The objective of this work is first to investigate if the final strip thickness relates to the amount of oxide formation.

In addition, the amount of oxide formation can affect the adhesion of scale to steel. This property is important. If the hot-rolled steel is delivered to the customer for the direct application in this form, good scale adhesion is required. If the hot-rolled has to be successively cold-rolled, the bad scale adhesion is preferred. This is because the scale can be easily removed from the steel surface before further cold rolling. The adhesion of oxide scale on steel substrate can be assessed in many ways, such as the indentation test [23], the inverted blister test [24, 25], the bending test [26-29] or the tensile test [30-34]. Our group developed the tensile test [35-39] to evaluate the scale adhesion of low carbon steels [15, 19,

* Corresponding author: thanasak.n@eng.kmutnb.ac.th

22, 35-39] and stainless steels [40-42]. It will be used in this study. The structure and adhesion of the oxide scale after the hot rolling process are focused on in this study. The effect of final strip thickness on scale formation and adhesion is emphasised. During the industrial production of steel, tons of iron-rich scale are produced as waste materials [43]. The waste contains large amounts of iron oxides, heavy metals and other different contaminants. It affects the environment when disposed of in landfills [44]. The environment is polluted. The scale as a process waste should be kept to a minimum.

For preventing scale formation in steel industries, since the scale formation during the hot rolling process at high temperatures. Several hot rolling conditions have been proposed to prevent the scale problem. Control of slab heating temperature and alloying elements content are some of those proposed processes. However, these conditions are not sufficient in preventing scale defects in the commercial hot rolling process. The thick scale formed during heating for a long time in the furnace and remains even after water jet descaling. A short time holding in the furnace might control this scale. The existence of fayalite (Fe_2SiO_4) for high Si steel is an additional important factor to prevent scale formation. This is due to scale thickness decreasing with the increasing silicon content. However, the strong bonding of fayalite on the scale-steel interface is considered to descaling process. The scale generated by the steel plant is called waste, but now this term has been replaced with a by-product. Mill scale is one of the by-products produced during steel processing. Mill scale is used for magnetic storage, polishing, chemical manufacturing, pigment manufacturing, and biomedical application.

2 Materials and methods

2.1 Materials

The study used hot-rolled steel which is available from Sahaviriya Steel Industries Public Company Limited as a strip with a thickness of 8, 10 and 12 mm. The position of the hot-rolled coil at the head, middle and tail are used for examination as shown in Figure 1. The sample is cut from a strip obtained from a slab produced by the blast-furnace route. In the hot rolling process, the finishing and coiling temperatures of the sample, which had a strip thickness of 8 mm are 790°C and 580°C respectively, for the strip 10 mm is 780°C and 590°C, for strip 12 mm is 760°C and 560°C.

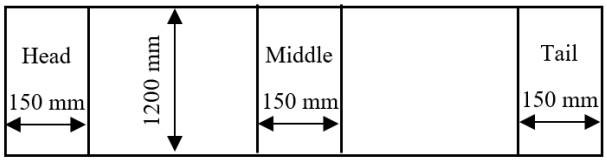

Figure 1. Position of sample in the hot-rolled coil taken for examination.

The hot-rolled steel is used for several products e.g. pipe and tube, automotive structural, machine structures, and gas cylinders. The final strip thickness is considered by product specification. Considered to phase transformation when exiting the hot rolling mill, the choice of finishing and coiling temperatures have a significant influence on achieving product property. Table 1 shows the chemical composition of the steel. Table 2 shows the information from mechanical tensile testing.

Table 1. Chemical composition of the as-received hot-rolled steel strip (wt.%).

Sample	C	Si	Cu	Mn	P	S
8 mm	0.138	0.006	0.010	0.441	0.017	0.009
10 mm	0.156	0.007	0.009	0.454	0.016	0.002
12 mm	0.158	0.009	0.007	0.440	0.020	0.006

Table 2. The tensile mechanical properties of a material.

Strip thickness	Mechanical properties		
	Yield strength (MPa)	Tensile strength (MPa)	Elongation (mm)
8 mm	444	502	18
10 mm	348	441	29
12 mm	385	463	27

2.2 Characterisation

The oxide scale morphology is observed by the scanning electron microscope (SEM, QUANTA 450). The energy-dispersive X-ray spectroscopy (EDS, OXFORD INSTRUMENTS, Model X-Max) was equipped with SEM for elemental analysis. The oxide phase is determined by the X-ray diffraction technique (XRD, SmartLab) using the Cu Kα line (k = 0.15406 nm) with a step size of 0.02 degree/step and a step time of 0.5 second/step.

2.3 Mechanical adhesion

The tensile testing machine (Instron, Model 5566) with a load of 10 kN is used. The strain rate of 0.04 s^{-1} at room temperature is operated. A high-magnification lens with a CCD camera has been used to observe the evolution of scale failure. The video processing is performed at a resolution of 640 × 480 pixels. Image framework programming is used to acquire the image. The CCD camera has a frame rate of 7.5 frames per second. The specimen is prepared according to the ASTM E8M standard. Figure 2 shows the tensile testing machine with the scale observation set and sample shape.

3 Results and discussion

Figure 3 presents cross sections of the 8-mm strip at the head, middle and tail positions. The XRD pattern for each scale was also shown in Figure 4. It was seen that the thickness of scale at the head position was 12.82 ± 2.57 μm. They were 16.42 ± 2.29 μm and 10.77 ± 1.15 μm at the middle and tail positions respectively. Fe_2O_3, Fe_3O_4 and Fe were found in the XRD patterns of the scale formed in these three positions. The literature [4] was reported the oxidation of iron and steel in oxygen or air at high temperatures. At temperatures above 700°C, iron

oxidation follows the parabolic law, resulting in the formation of three-layered hematite, magnetite, and wustite. Carbon steel oxidation was generally slower than iron oxidation. The scale structure of carbon steel was similar to those formed on iron after very short-term oxidation.

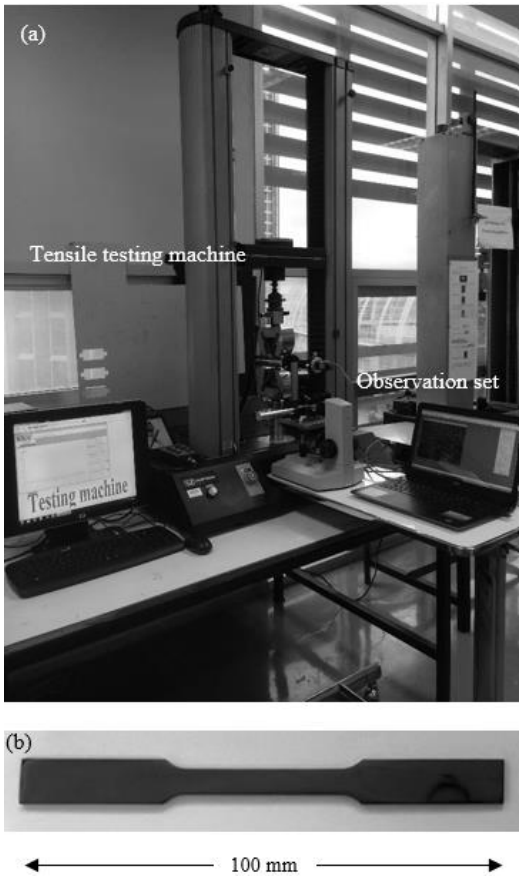

Figure 2. Tensile machine set up with observation set (a) and sample shape (b).

The oxidation behaviour of carbon steel at high temperatures has been extensively studied in the previous. Oxidation behaviour of steel and scale structure was more difficult to understand than iron oxidation due to the presence of various alloying and impurity elements. However, literature [45] has proposed that the steam partial pressure was unaffected by the rate of oxidation. The hematite layer was very thin, which affects the oxygen activity at the magnetite-hematite interface. From this research, hematite and magnetite layers were observed without the wustite layer. According to the Fe-O phase diagram as shown in Figure 5, wustite will fully decompose undergoes eutectoid transformation and turns into magnetite and iron at 570°C or below during the cooling after hot rolling. Literature [20] suggestion was a direct magnetite-formation mechanism. The presence of an iron substrate was not essential for the formation of the magnetite layer. The mechanism of forming the magnetite layer was via the following primary reaction without the involvement of the iron base.

$$Fe_{1-x}O \rightarrow [(x-y)/(1-4y)]Fe_3O_4 + [(1-4x)/(1-4y)]Fe_{1-y}O \quad (1)$$

where $Fe_{1-y}O$ is an iron-rich wustite, which subsequently decomposed into a eutectoid product via the following reaction.

$$4Fe_{1-y}O \rightarrow Fe_3O_4 + (1-4y)Fe \quad (2)$$

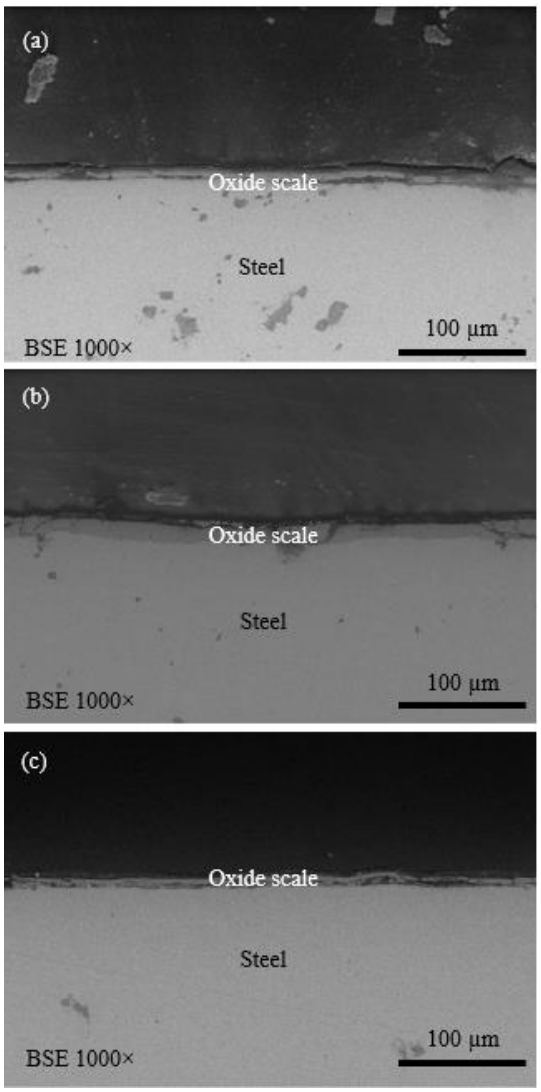

Figure 3. Scale structures on a strip with 8 mm of thickness at head (a), middle (b) and tail (c) positions.

During wustite decomposition, primary magnetite precipitation inside the wustite phase was readily formed and then followed by magnetite precipitation at the wustite-iron interface. Finally, eutectoid forming magnetite and iron. In our view, high temperature promoted the development of the wustite layer which was possible at temperatures higher than 570°C. At temperatures below 570°C, the layered magnetite and iron eutectoid were continuously formed. Conversely, wustite could be found at temperatures below 570°C when the cooling rate was high enough. In addition, wustite might undergo a eutectoid reaction to form a mixture of magnetite and iron when oxidation was preceded under a continuous cooling process. The oxide scale microstructure formed via phase transformation of wustite affects the surface quality of steel products. However, this study was focused on the effect of final strip thickness in

the simplest way for understanding the adhesion of iron oxide waste scale from the rolling mill steel industry. Therefore, it was necessary to have a good understanding of oxide scale composition. Table 3 shows the composition of the oxide scale obtained from hot-rolled steel. The EDS mapping spectra for the sample shows that the main elemental components were Fe, O and C. This indicates that the iron oxide as the main phase was presented, and the carbon-rich originate from the hot-rolled steel. It can be noted that the presence of Si was found on a scale of a 10 mm strip thickness at the middle position. It was due to Si-rich precipitates in the oxide scale of their steel.

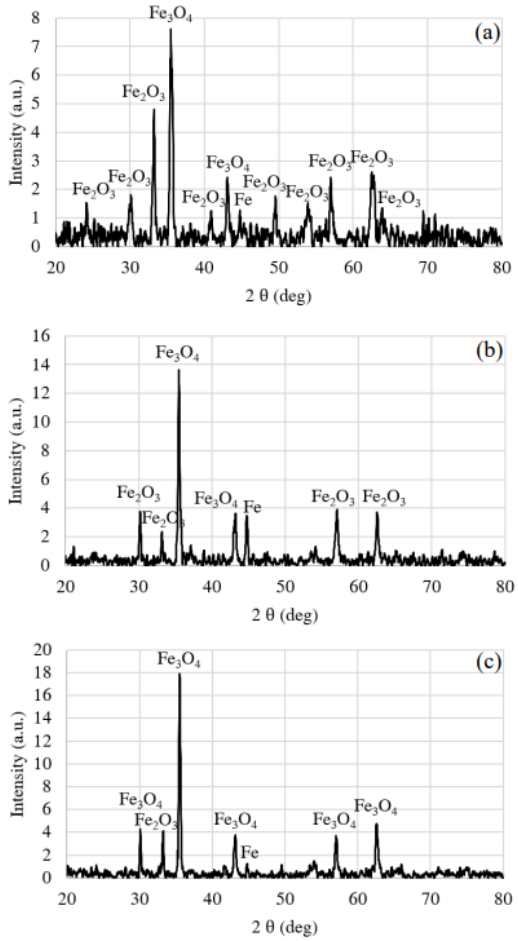

Fig. 4. XRD patterns of the strip with 8 mm of thickness at the head (a), middle (b) and tail (c) positions.

Table 3. Elemental quantification in percentage weight (wt.%) obtained by EDS analysis for the scale as-received hot-rolled steel strip.

Thick	Position	Fe	O	C	Si
8 mm.	Head	40.26	23.74	36.00	
	Middle	37.59	30.22	32.20	
	Tail	34.75	31.43	33.81	
10 mm.	Head	21.64	33.64	42.45	
	Middle	38.76	38.08	22.02	1.13
	Tail	37.49	35.37	25.65	
12 mm.	Head	43.26	23.31	33.44	
	Middle	40.33	34.00	25.67	
	Tail	39.91	37.26	22.82	

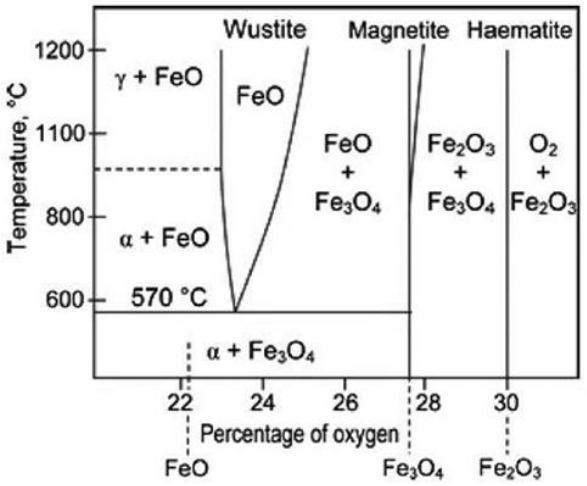

Figure 5. Fe-O phase diagram [46].

Figure 6 illustrates cross sections of the 10-mm strip at the head, middle and tail positions. The XRD pattern for each scale was also shown in Figure 7. It was seen that the thickness of scale at the head position was 10.41 ± 3.89 μm. They were 37.44 ± 7.61 μm and 13.34 ± 3.34 μm at the middle and tail positions respectively. Fe_2O_3, Fe_3O_4 and Fe were found in the XRD patterns of the scale formed in these three positions.

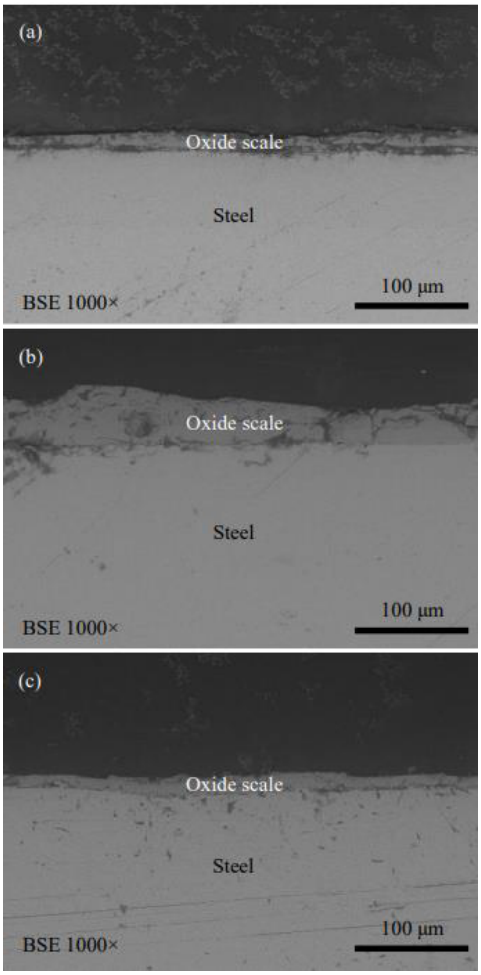

Figure 6. Scale structures on a strip with 10 mm of thickness at the head (a), middle (b) and tail (c) positions.

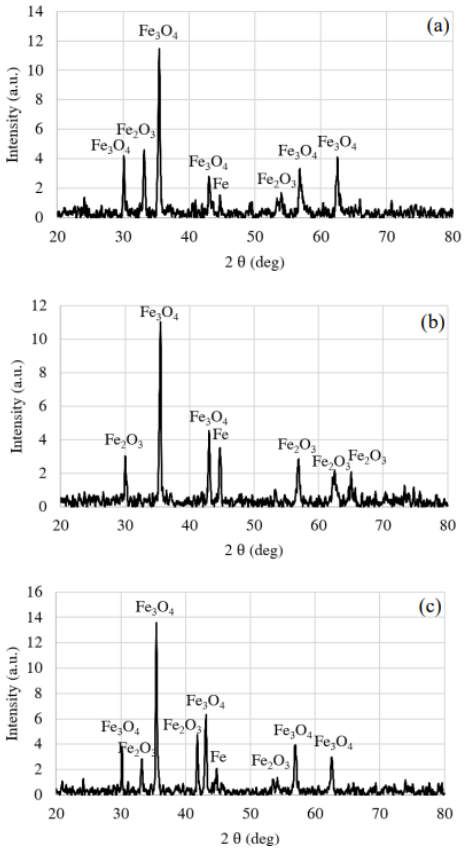

Figure 7. XRD patterns of the strip with 10 mm of thickness at head (a), middle (b) and tail (c) positions.

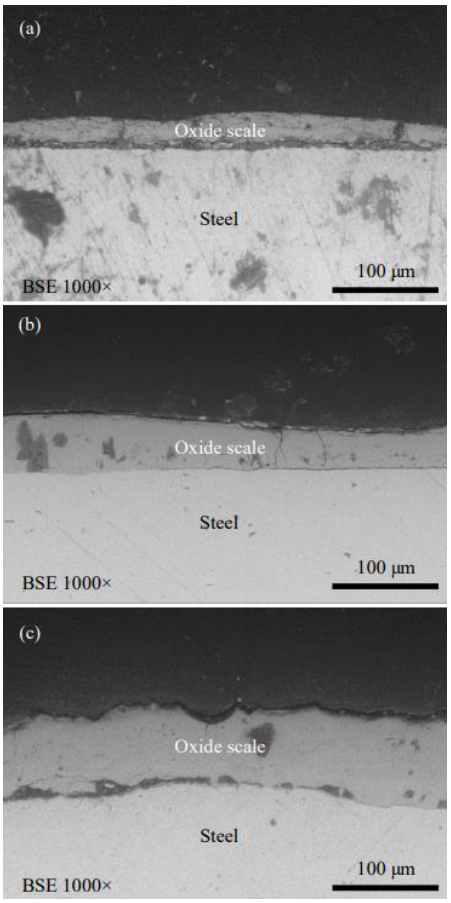

Figure 8. Scale structures on a strip with 12 mm of thickness at the head (a), middle (b) and tail (c) positions.

Figure 8 shows cross sections of the 12-mm strip at the head, middle and tail positions. The XRD pattern for each scale was also shown in Figure 9. It was seen that the thickness of scale at the head position was 29.44 ± 2.63 µm. They were 45.13 ± 8.99 µm and 74.36 ± 6.54 µm at the middle and tail positions respectively. Fe_2O_3, Fe_3O_4 and Fe were found in the XRD patterns of the scale formed in these three positions.

From XRD results, the oxide scale formed at rolling temperatures comprises hematite and magnetite with iron as shown in all samples. Qualitative phase analysis provides oxide scale information gleaned from an X-ray diffraction pattern. Each phase of a crystalline oxide will produce a unique diffraction pattern. The diffracted peak positions and intensities from a particular oxide phase serve as a fingerprint that can be compared to a database of reference patterns to identify a phase. A pattern plot of diffracted X-ray intensity with Bragg angle. The peak positions of the hematite phase shown at 24.17°, 33.19°, 35.66°, 40.90°, 49.51°, 54.13°, 62.49°, and 64.05° were indexed to (012), (104), (110), (113), (024), (116), (214), and (300) respectively. While the peak positions of the magnetite phase shown at 30.07°, 35.42°, 43.05°, 56.93°, and 62.51° were indexed to (220), (311), (400), (511), and (440) respectively. The peak positions of the iron phase shown at 44.68°, 65.03°, and 82.34° were indexed to (110), (200), and (211) respectively. It can be noted that the peak positions and relative intensities of the sharp peaks in XRD patterns indicate the hematite, magnetite and iron were well crystallised.

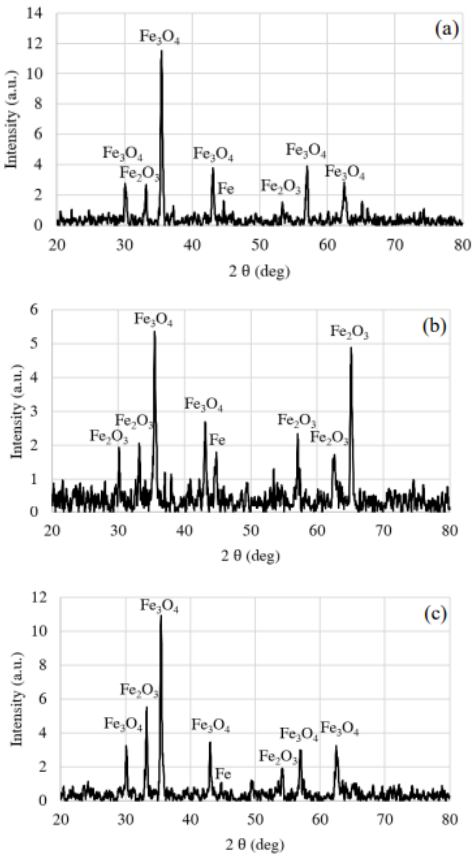

Figure 9. XRD patterns of the strip with 12 mm of thickness at head (a) position middle (b) and tail (c) positions.

A comparison of the oxide scale thickness as a function of final strip thickness for specimens at the position of the head, middle and tail was shown in Figure 10. The thickness was measured using cross-sectional metallographic images. It was found that the scale thickness of the studied 12-mm thick strip was significantly increased at all positions. It was well known that the thickness of oxide scale was linear with the weight gain of the scale due to the absorption of oxygen. With the increase in exposure time, the internal and external thickness of the oxide scale gradually thickens. If the strip thickness is high, provide more time for cooling after the hot rolling process. Scale continued to grow as a result. It was also seen that the thickness at the tail position on a strip of 12 mm was higher than that head and middle positions. This might be due to the accumulation of heat at the strip tail during the hot rolling process, corresponding to using a longer cooling time. The results indicate a drop in scale thickness when the final strip thickness was decreased. This can be attributed to the higher cooling rate of the thinner strip. While the scale thickness at the middle position on strips of 8mm and 10mm seems to be higher than the head and tail positions. Literature [47], this study was to improve the longitudinal performance uniformity of hot-rolled coils. The results show that the average cooling rate of the head and tail parts were higher than that of the middle part during coil cooling. This might cause lower scale thickness on strips of 8-mm and 10-mm at head and tail positions. However, accumulation of heat at the strip tail was going to have an effect on the strip of 12 mm. It can be observed that the global scale thickness of the strip of 12 mm seems to be higher.

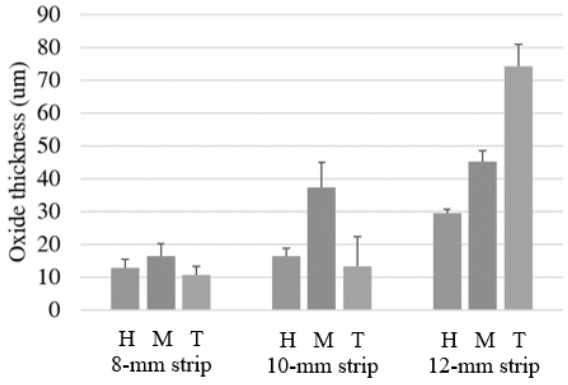

Figure 10. Oxide scale thickness of strip with 8, 10 and 12 mm of thickness at the head (H), middle (M) and tail (T) positions.

Comparison literature [48], this research shows the thicknesses of oxides formed on AISI 1045 were 2.92 µm and 6.22 µm for oxidation of 168 and 720 hours respectively. Oxidation of steel was performed in the heated air inside the furnace at 673 K (400°C). After the oxidation process was completed, the sample was kept in a desiccator for cooling down to room temperature. Note that before oxidation the steel was cut into 20 mm in diameter with a thickness of 2 mm. The results show that the scale thickness was found in the range of 3-6 µm, this lower than that scale thickness was observed on as-received hot-rolled steel with a final strip thickness of 8-12 mm. This was due to the difference between the thickness of the sample, oxidation temperature and oxidation time.

The oxide adhesion to a steel substrate will be discussed formally in terms of oxide-steel separation. The adhesion of scale on steel was previously considered [49]. Many failures occurred in the oxide near the interface, involving oxide growth stresses, oxide and steel plasticity, and thermal cycle effects caused by differential thermal contraction. Cracks normal to the interface, cracks parallel to the interface or spalling were all examples of local failures. Attention was focused here on the scale spallation and adhesion. Figure 11 shows strain initiating the first spallation of the strip with 8, 10 and 12 mm of thickness at the head, middle and tail positions. It was seen that the strain resulting induced the first spallation of a strip with a thickness of 12 mm was lower at all positions. This indicates that during the hot rolling process oxide scale was easier to flake off. In terms of mechanical adhesion energy, it was determined using information from the literature [26, 50-54]. The values reveal that the strip with a thickness of 12 mm has lower mechanical adhesion energy at all positions as shown in Figure 12.

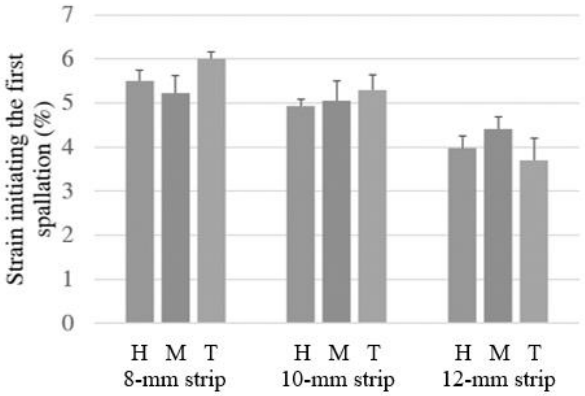

Figure 11. Strain initiating the first spallation of the strip with 8, 10 and 12 mm of thickness at the head (H), middle (M) and tail (T) positions.

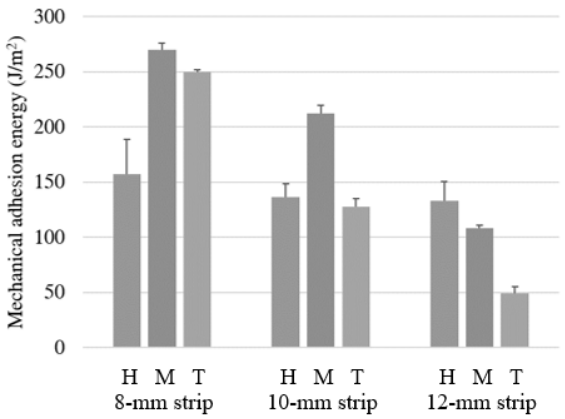

Figure 12. Mechanical adhesion energy of strip with 8, 10 and 12 mm of thickness at the head (H), middle (M) and tail (T) positions.

The scale adhesion was increased with decreasing final strip thickness. This was confirmed by the result in Figure 11. It was seen that the strain initiating the first spallation tends to be lower for the 12-mm sample. It was reported in the literature that the higher scale thickness tends to be lower strain initiating the first spallation [25, 52-53]. This was because if metals diffuse from the internal steel-scale interface to the external scale-gas interface, voids can be formed at the scale-steel interface [55]. The thinner scale had a lower diffusing rate of metal to the external interface, and therefore voids should be less. Then the adhesion should be better. The thinner strip should be pressed more during the rolling. This process might change the properties of the scale and the steel-scale interface strength in a way that increased the scale adhesion. During the hot rolling process, oxide scale spallation was always a possibility. Among the waste from the steelmaking industry, iron oxide produces millions of tons resulting in pollution to the environment. To protect the environment, it was necessary to treat steel waste carefully. Literature [56] was reported the characterisation of iron oxide waste scale obtained by the rolling mill steel industry. The oxide sample revealed α-Fe_2O_3 (hematite) and Fe_3O_4 (magnetite) as principal and secondary phases. It was important to have a good understanding of the relationship between scale structure and strip thickness conditions because the oxide structure had a significant impact on the descaling performance of hot rolled steel strip [57]. It was well known that the pickling process was easier on wustite than that on magnetite [57-59].

4 Conclusion

Formation of thermal oxide scale and its adhesion to hot-rolled low carbon steel with different final strip thicknesses was studied. The purpose of this study was on scale failure in relation to waste scale. The following conclusions could be drawn:

4.1 The strain initiation of the first spallation and adhesion energy of oxide formed on 12 mm strip thickness was found to be lower, causing oxide scale to spall easily.

4.2 More oxide thickness and lower adhesion of scale on hot-rolled steel with 12 mm strip thickness resulted in increased iron oxide waste scale obtained by the rolling mill steel industry.

4.3 The present work studied the only effect of final strip thickness on oxide scale formation and its adhesion to hot-rolled steel. The effect of final strip thickness on adhesion of scale on steel substrate should further be investigated by the pickling test or other methods e.g. the indentation test for comparison.

Acknowledgements

This research was funded by National Science, Research and Innovation Fund (NSRF), and King Mongkut's University of Technology North Bangkok with Contract no. KMUTNB-FF-65-09. Sahaviriya Steel Industries Public Company Limited for the provision of the hot-rolled steel strip.

References

1. P. Kofstad, *High temperature corrosion* (Elsevier Applied Science, London, UK, 1988)
2. R.Y. Chen, W.Y.D. Yuen, Oxide-scale structures formed on commercial hot-rolled steel strip and their formation mechanisms, Oxidation of Metals, 56, 1/2, (2001): 89-118
3. R.Y. Chen, W.Y.D. Yuen, Oxidation of low-carbon, low-silicon mild steel at 450-900°C under conditions relevant to hot-strip processing, Oxidation of Metals, 57, 1/2, (2002): 53-79
4. R.Y. Chen, W.Y.D. Yuen, Review of the high-temperature oxidation of iron and carbon steels in air or oxygen, Oxidation of Metals, 59, 5/6, (2003): 433-468
5. R.Y. Chen, W.Y.D. Yuen, Examination of oxide scales of hot rolled steel products, Iron and Steel Institute of Japan International, 45, 1, (2005): 52-59
6. P. Sarrazin, A. Galerie, J. Fouletier, *Les mécanismes de la corrosion sèche: une approche cinétique* (EDP Science, France, 2000)
7. P. Sarrazin, A. Galerie, J. Fouletier, *Mechanisms of high temperature corrosion: a kinetic approach* (Materials Science Foundations, Trans Tech Publications, Stafa-Zürich, Switzerland, 2008)
8. M.J.L. Gines, G.J. Benitez, T. Perez, E. Merli, M.A. Firpo, W. Egli, Study of the picklability of 1.8 mm hot-rolled steel strip in hydrochloric acid, Latin American Applied Research, (2002): 281-288
9. Z.Y. Jiang, A.K. Tieu, W.H. Sun, J.N. Tang, D.B. Wei, Characterisation of thin oxide scale and its surface roughness in hot metal rolling, Materials Science and Engineering A, 435-436, (2006): 434-438
10. L. Suárez, R. Petrov, L. Kestens, M. Lamberigts, Y. Houbaert, Texture evolution of tertiary oxide scale during steel plate finishing hot rolling simulation tests, Materials Science Forum, 550, (2007): 557-562
11. M. Zhang, G. Shao, Characterization and properties of oxide scales on hot-rolled strips, Materials Science and Engineering A, 452-453, (2007): 189-193
12. Y.-L. Yang, C.-H. Yang, S.-N. Lin, C.-H. Chen, W.-T. Tsai, Effects of Si and its content on the scale formation on hot-rolled steel strips, Materials Chemistry and Physics, 112, (2008): 566-571
13. A. Segawa, Reproduction and deformation characteristics of oxide scale in hot rolling using vacuum rolling mill, Materials Science Forum, 696, (2011): 150-155
14. V.B Ginzburg, *Flat-rolling fundamentals* (New York: Marcel Dekker, Inc. 2000)
15. S. Chandra-ambhorn, T. Phadungwong, K. Sirivedin, Effects of carbon and coiling temperature on the adhesion of thermal oxide scales to hot-rolled carbon steels, Corrosion Science, 115, (2017): 30-40
16. S. Chandra-ambhorn, T. Nilsonthi, Y. Wouters, A. Galerie, Oxidation of simulated recycled steels with 0.23 and 1.03 wt.% Si in Ar–20% H_2O at 900°C, Corrosion Science, 87, (2014): 101-110

17. R.Y. Chen, W.Y.D. Yuen, Isothermal and step isothermal oxidation of copper-containing steels in air at 980-1220°C, Oxidation of Metals, 63, 3/4, (2005): 145-168
18. S. Chandra-ambhorn, A. Jutilarptavorn, T. Rojhirunsakool, High temperature oxidation of irons without and with 0.06 wt.% Sn in dry and humidified oxygen, Corrosion Science, 148, (2019): 355-365
19. S. Chandra-ambhorn, K. Ngamkham, High temperature oxidation of micro-alloyed steel and its scale adhesion, Oxidation of Metals, 88, (2017): 291-300
20. R.Y. Chen, W.Y.D. Yuen, A study of the scale structure of hot-rolled steel strip by simulated coiling and cooling, Oxidation of Metals, 53, 5/6, (2000): 539-560
21. R.Y. Chen, W.Y.D. Yuen, Copper enrichment behaviours of copper-containing steels in simulated thin-slab casting processes, Iron and Steel Institute of Japan International, 45, 6, (2005): 807-816
22. S. Chandra-ambhorn, K. Ngamkham, N. Jiratthanakul, Effects of process parameters on mechanical adhesion of thermal oxide scales on hot-rolled low carbon steels, Oxidation of metals, 80, 1, (2013): 61-72
23. J.L. Beuth, N. Dhanaraj, J. Hammer, S. Laney, F.S. Pettit, G.H. Meier, *ASM Materials Solutions Conference and Show* (Columbus, OH, October 18-24, 2004)
24. J. Mougin, M. Dupeux, A. Galerie, L. Antoni, Inverted blister test to measure adhesion energy of thermal oxide scales on metals or alloys, Materials Science and Technology, 18, 10, (2002): 1217-1220
25. J. Mougin, M. Dupeux, L. Antoni, A. Galerie, Adhesion of thermal oxide scales grown on ferritic stainless steels measured using the inverted blister test, Materials Science and Engineering A, 359, (2003): 44-51
26. A. Galerie, F. Toscan, E. N'Dah, K. Przybylski, Y. Wouters, M. Dupeux, Measuring adhesion of Cr_2O_3 and Al_2O_3 scales on Fe-based alloys, Materials Science Forum, 461-464, (2004): 631-638
27. M.M. Nagl, W.T. Evans, D.J. Hall, S.R.J. Saunders, The failure of iron oxide scales at growth temperature under tensile stress, Journal de Physique IV, 3, (1993): 933-941
28. M.M. Nagl, S.R.J. Saunders, W.T. Evans, D.J. Hall, The tensile failure of nickel oxide scales at ambient and at growth temperature, Corrosion Science, 35, 5-8, (1993): 965-977
29. M.M. Nagl, W.T. Evans, D.J. Hall, S.R.J. Saunders, An in situ investigation of the tensile failure of oxide scales, Oxidation of Metals, 42, (1994): 431-449
of AISI 430 stainless steel in O2-40%H_2O at 800°C, Corrosion Science, 203, (2022)
43. M.Z. Ruhiyuddin, D. Murizam, K.R. Ahmad, Synthesis and characterization of iron produced from iron mill scale, Key Engineering Materials, 594–595, (2014): 118-122
30. M. Krzyzanowski, J.H. Beynon, The tensile failure of mild steel oxides under hot rolling conditions, Steel Research, 70, (1999): 22-27
31. M. Krzyzanowski, J.H. Beynon, Finite element model of steel oxide failure during tensile testing under hot rolling conditions, Materials Science and Technology, 15, 10, (1999): 1191-1198
32. M. Krzyzanowski, J.H. Beynon, C.M. Sellars, Analysis of secondary oxide-scale failure at entry into the roll gap, Metallurgical and Materials Transactions B, 31, 6, (2000): 1483-1490
33. D. Geneve, D. Rouxel, P. Pigeat, M. Confente, Descaling ability of low-alloy steel wires depending on composition and rolling process, Corrosion Science, 52, (2010): 1155-1166
34. Y.T. Chiu, C.K. Lin, J.C. Wu, High-temperature tensile and creep properties of a ferritic stainless steel for interconnect in solid oxide fuel cell, Journal of Power Sources, 196, (2011): 2005-2012
35. K. Ngamkham, S. Niltawach, S. Chandra-ambhorn, Development of tensile test to investigate mechanical adhesion of thermal oxide scales on hot-rolled steel strips produced using different finishing temperatures, Key Engineering Materials, 462-463, (2011): 407-412
36. S. Chandra-ambhorn, N. Klubvihok, Quantification of adherence of thermal oxide scale on low carbon steel using tensile test, Oxidation of Metals, 85, 1, (2016): 103-125
37. T. Nilsonthi, W. Issaard, S. Chandra-Ambhorn, Development of the scale adhesion assessment using a tensile testing machine equipped with a CCD camera, Oxidation of Metals, 88, (2017): 41-55
38. W. Issaard, T. Nilsonthi, Application of the tensile test with a CCD camera to assess the adhesion of scale to Si-containing hot-rolled steels, Key Engineering Materials, 728, (2017): 26-30
39. N. Na-kalasin, S. Yenchum, T. Nilsonthi, Adhesion behaviour of scales on hot-rolled steel strips produced from continuous casting slabs, Materials Today: Proceedings, 5, (2018): 9359-9367
40. S. Chandra-ambhorn, P. Saranyachot, T. Thublaor, High temperature oxidation behaviour of Fe-15.7 wt.% Cr-8.5 wt.% Mn in oxygen without and with water vapour at 700°C, Corrosion Science, 148 (2019): 39-47
41. S. Chandra-ambhorn, T. Thublaor, P. Wiman, High temperature oxidation of AISI 430 stainless steel in Ar-H_2O at 800°C, Corrosion Science, 167, (2020)
42. P. Wiman, T. Thublaor, T. Rojhirunsakool, M.H.S. Bidabadi, Z.G. Yang, T. Siripongsakul, W. Chandra-ambhorn, S. Chandra-ambhorn, Corrosion behaviour
44. S.R. Prim, M.V. Folgueras, M.A. de Lima, D. Hotza, Synthesis and characterization of hematite pigment obtained from a steel waste industry, Journal of Hazardous Materials, 192, (2011): 1307-1313
45. N.J. Cory, T.M. Herrington, The location of hydrogen in the kinetics of oxidation of ferrous alloys

by superheated steam, Oxidation of Metals, 29, 1-2, (1988): 135-152
46. A.S. Khanna, *Introduction to high temperature oxidation and corrosion* (Ohio, ASM International, 2004)
47. H. Li, T. Li, C. Li, Z. Wang, G. Wang, Improvement of longitudinal performance uniformity of hot-rolled coils for cold-rolled DP980 steel, Metals, 10, (2020): 1-14
48. H. Krungkarnchana, C. Kongvarhodom, Low temperature corrosion: oxidation of carbon steel and stainless steel in air, Applied Science and Engineering Progress, 12, 1, (2019): 44-51
49. G.C. Wood, J. Stringer, The adhesion of growing oxide scales to the substrate, Journal de Physique IV, 3, (1993): 65-74
50. F. Toscan, L. Antoni, Y. Wouters, M. Dupeux, A. Galerie, Oxidation kinetics and scale spallation of iron-chromium alloys with different titanium contents, Materials Science Forum, 461-464, (2004): 705-712
51. S. Chandra-ambhorm, F. Roussel-Dherbey, F. Toscan, Y. Wouters, A. Galerie, M. Dupeux, Determination of mechanical adhesion energy of thermal oxide scales on AISI 430Ti alloy using tensile test, Materials Science and Technology, 23, 4, (2007): 497-501
52. G. Bamba, Y. Wouters, A. Galerie, F. Charlot, A. Dellali, Thermal oxidation kinetics and oxide scale adhesion of Fe-15Cr alloys as a function of their silicon content, Acta Materialia, 54, (2006): 3917-3922
53. S. Chandra-ambhorn, Y. Wouters, L. Antoni, F. Toscan, A. Galerie, Adhesion of oxide scales grown on ferritic stainless steels in solid oxide fuel cells temperature and atmosphere conditions, Journal of Power Sources, 171, (2007): 688-695
54. T. Nilsonthi, Determination of mechanical adhesion energy of thermal oxide scales on steel produced from medium and thin slabs using tensile test, Key Engineering Materials, 658, (2015): 106-110
55. H.E. Evans, Stress effects in high temperature oxidation of metals, International Materials Reviews, 40, 1, (1995): 1-40
56. J. Kargin, L.L.S. Valladares, L.E. Borja-castro, J. Xize, D.G. Mukhambetov, Y. V. Konyukhov, N.O. Moreno, A.G.B. Dominguez, C.H.W. Barnes, Characterization of iron oxide waste scales obtained by rolling mill steel industry, Hyperfine Interactions, 243, (2022): 1-10
57. J. Tominaga, K. Wakimoto, T. Mori, M. Murakami, T. Yoshimura, Manufacture of wire rods with good descaling property, Transactions of the Iron and Steel Institute of Japan, 22, 8, (1982): 646-656
58. S. Garber, Fundamental aspects of scale on mild steel strip, Journal of the Iron and Steel Institute, 192, (1959): 153-160
59. K. Sachs, G.T.F. Jay, A magnetic seam at the scale/metal interface on mild steel, Journal of the Iron and Steel Institute, 195, (1960):180-189